Biogeosciences Discuss., https://doi.org/10.5194/bg-2019-103
Manuscript under review for journal Biogeosciences
Discussion started: 26 March 2019

Biogeosciences
Discussions
Open Access

Air–Sea Fluxes of Greenhouse Gases and Oxygen in the Northern Benguela Current Region During Upwelling Events

Eric J. Morgan[1,2], Jost V. Lavric[1], Damian L. Arévalo-Martínez[3], Hermann W. Bange[3], Tobias Steinhoff[3], Thomas Seifert[1], and Martin Heimann[1,4]

[1]Max Planck Institute for Biogeochemistry, Jena, Germany
[2]Now at: Scripps Institution of Oceanography, La Jolla, CA, U.S.A.
[3]GEOMAR Helmholtz Centre for Ocean Research, Kiel, Germany
[4]Institute for Atmospheric and Earth System Research (INAR) / Physics, University of Helsinki, Finland

Correspondence: Eric J. Morgan (ejmorgan@ucsd.edu)

Abstract. Ground-based atmospheric observations of CO_2, $\delta(O_2/N_2)$, N_2O, and CH_4 were used to make top-down estimates of the air–sea fluxes of these species from the Lüderitz and Walvis Bay upwelling cells in the northern Benguela region, during upwelling events. Average flux densities ($\pm 1\sigma$) were 0.64 ± 0.4 μmol m^{-2} sec^{-1} for CO_2 , -5.1 ± 1.4 μmol m^{-2} sec^{-1} for O_2 (as APO), 0.57 ± 0.3 nmol m^{-2} sec^{-1} for N_2O, and 4.3 ± 5.5 nmol m^{-2} sec^{-1} for CH_4. A comparison of our top-down flux estimates with shipboard-based measurements showed good agreement between both approaches. During the study, upwelling events were sources of CO_2, N_2O, and CH_4 to the atmosphere. N_2O fluxes were fairly low, in accordance with previous work suggesting that the evasion of this gas from the Benguela is smaller than for other Eastern Boundary Upwelling Systems (EBUS). Conversely, CH_4 release was quite high for the marine environment, a result that supports studies that indicated a large sedimentary source of CH_4 in the Walvis Bay area. These results demonstrate the suitability of atmospheric time series for characterizing the temporal variability of upwelling events and their influence on the overall marine GHG emissions from the northern Benguela region.

1 Introduction

Coastal margins, particularly those associated with the upwelling of nutrient-rich subsurface waters, are biogeochemically active regions (Levin et al., 2015). The air–sea fluxes of greenhouse gases (GHGs; referring to the long-lived greenhouse gases CO_2, N_2O, and CH_4) from or to such systems can vary markedly, both spatially and temporally (Torres et al., 1999; Naqvi et al., 2010; Evans et al., 2011; Reimer et al., 2013; Capone and Hutchins, 2013). This is because the occurrence and intensity of coastal upwelling events are episodic in nature, as they are forced by surface winds that occur under specific synoptic conditions; even large events happen only on a time scale of days (Blanke et al., 2005; Goubanova et al., 2013; Desbiolles et al., 2014a, b). The sporadic nature of upwelling implies that observations made during short-term campaigns may not capture the full range of flux variability.

Upwelled water is usually colder than the surrounding surface water, which means that the solubility of dissolved gases will decrease with increasing temperature as water masses warm at the surface. A competing influence for CO_2 exists in

Biogeosciences Discuss., https://doi.org/10.5194/bg-2019-103
Manuscript under review for journal Biogeosciences
Discussion started: 26 March 2019

that the supply of inorganic nutrients from an upwelling event can lead to blooms of phytoplankton and a net drawdown of atmospheric CO_2. For O_2, the ventilation of deeper water masses can drive a net flux into the ocean, or net productivity can create oversaturation of dissolved O_2. Hence, coastal upwelling regions can oscillate between being sources and sinks of O_2 and CO_2 (Torres et al., 1999; Santana-Casiano et al., 2009; González-Dávila et al., 2009; Gregor and Monteiro, 2013; Cao et al., 2014; Evans et al., 2015). Most coastal upwelling systems are also known to be regional hotspots of N_2O emissions (Bange et al., 2001; Lueker et al., 2003; Cornejo et al., 2006; Bianchi et al., 2012; Arévalo-Martínez et al., 2015; Babbin et al., 2015). Air-sea fluxes of CH_4 are less constrained, but may be a significant term in the marine CH_4 budget (Rehder et al., 2002; Sansone et al., 2001).

A well-established method of estimating yearly budgets of air–sea fluxes for GHGs in upwelling regions is to take wind fields and interpolated or representative surface measurements, use them to calculate a flux density, and scale it up over a selected area. The high variability of air–sea exchange means that determining yearly budgets of air–sea fluxes of GHGs is challenging without a high degree of spatial and temporal sampling.

Another approach, and one that sidesteps some of these difficulties, is to use a top-down method, *i.e.*, using atmospheric measurements to infer fluxes from the surface, using simple models (Lueker et al., 2003; Lueker, 2004; Nevison et al., 2004; Thompson et al., 2007; Yamagishi et al., 2008) or more complex inverse methods (*e.g.*, Rödenbeck et al. (2008)). A simple top-down approach has been successfully employed to detect air–sea fluxes of CO_2, O_2, and N_2O from the California Current region from a coastal atmospheric monitoring station at Trinidad Head, California (Lueker et al., 2003; Lueker, 2004; Nevison et al., 2004). This work motivated our own efforts to see if anomalies related to upwelling events could be seen in continuous observations from an atmospheric measurement site located near the upwelling region in the northern Benguela, which is one of the least sampled EBUS for air–sea fluxes of GHGs (Nevison et al., 2004; Naqvi et al., 2010; Laruelle et al., 2014).

In this study, two years of continuous observations from a ground-based atmospheric observatory for greenhouse gases, the Namib Desert Atmospheric Observatory (NDAO), were utilized to create top-down estimates of the air–sea flux densities of CO_2, O_2, N_2O, and CH_4 from the Lüderitz and Walvis Bay upwelling cells. This area of the coastal shelf, stretching from ca. 22°S to 28°S, is subject to the strongest surface winds and upwelling fluxes of water in the region, and surface chlorophyll is at a minimum (Lutjeharms and Meeuwis, 1987; Hagen et al., 2001; Demarcq et al., 2007; Veitch et al., 2009; Hutchings et al., 2009). These estimates were then compared with shipboard measurements from a cruise in the two upwelling centers.

2 Methods

2.1 Atmospheric Measurements at the Namib Desert Atmospheric Observatory

Continuous measurements of CO_2, atmospheric oxygen, N_2O, CH_4, and CO were made at the Namib Desert Atmospheric Observatory (NDAO), a background site located at 23.563°S, 15.045°E, in the central Namib Desert, at Gobabeb Research and Training Centre. A full description of the measurement system is given in Morgan et al. (2015). In brief, observations were made at 21 m height above ground level with a Picarro ESP-1000 cavity ringdown spectrometer for CO_2 and CH_4, a Los Gatos N_2O/CO-23d cavity-enhanced absorption spectrometer for N_2O and CO, and an Oxzilla FC-II dual absolute and differential oxygen analyzer for $\delta(O_2/N_2)$. The average uncertainty for each species during the study period was 0.028 ppm for CO_2, 6.5 per meg for $\delta(O_2/N_2)$, 0.21 ppb for N_2O, 0.17 ppb for CH_4, and 0.15 ppb for CO. CO_2, N_2O, CH_4, and CO are all expressed as dry air mole fractions, in ppb or ppm (1 ppm = 1 μmol mol^{-1}; 1 ppb = 1 nmol mol^{-1}).

Atmospheric oxygen was quantified relative to atmospheric N_2, in per meg units (Keeling and Shertz, 1992):

$$\delta(\mathrm{O_2/N_2}) = \left(\frac{(\mathrm{O_2/N_2})_{sample}}{(\mathrm{O_2/N_2})_{ref}} - 1\right) \times 10^6 \qquad (1)$$

A data-derived tracer has been standardized to remove the influence of terrestrial photosynthesis and respiration on atmospheric oxygen, known as atmospheric potential oxygen (APO). APO is defined as as:

$$\mathrm{APO} = \delta(\mathrm{O_2/N_2}) + \frac{1.1}{\mathrm{X_{O_2}}}(\mathrm{CO_2} - 350) \qquad (2)$$

Here 1.1 is the nominal global average oxidative ratio (OR; $\Delta O_2/\Delta CO_2$ on a mol/mol basis) for terrestrial photosynthesis and respiration (Severinghaus, 1995), X_{O_2} is the mole fraction of oxygen in the atmosphere, 0.209392 (Tohjima et al., 2005). 350 is a reference CO_2 value, CO_2 is the in situ concentration of carbon dioxide, in ppm. APO and $\delta(O_2/N_2)$ are both expressed in per meg (Stephens et al., 1998). In some instances it is useful to express APO in molar units that are of the same relative magnitude as the dry air mole fraction in ppm. This conversion is done by multiplying $\delta(O_2/N_2)$ or APO by X_{O_2}. We refer to this unit as parts per million equivalents, or "ppm eq".

2.2 Identification of Upwelling Events and Selection of Atmospheric Anomalies

A subset of the coastal region was selected to represent the Lüderitz and Walvis Bay upwelling cells. The boundaries of this domain were at 13°E, 15°E, 23°S, and 27°S (Figure 1, *right panel*), representing an ocean area of 56,196 km^2. This domain covers the continental shelf and a small portion of the continental slope; the mean water depth is 390 m.

Upwelling events were identified based on sea surface temperature (SST) and 10 m wind speed anomalies. An event was determined to occur if the average deseasonalized SST of the domain was 0.5°C or lower than a smoothed, second-degree polynomial fit to the entire time series, and the average 10 m wind speed of the study area was 2.5 m sec^{-1} above a smoothed, second-degree polynomial fit to the wind data. These thresholds were arrived at through visual inspection of maps and time series of SST and wind speed data, and are specific to the domain chosen, since the data considered were averages of the entire area. Since the resolution of the SST and wind speed time series was daily, all higher resolution data falling within a day during which an upwelling event occurred was similarly flagged.

Atmospheric anomalies associated with upwelling events were quantified against a baseline determined through a second-harmonic fit that was generated iteratively to all data, excluding all points that lay outside 1 standard deviation from the curve for the subsequent iteration. Small adjustments were made to the anomaly to raise or lower the curve in cases where it did not intersect with background values within ± 5 days of the event. The NDAO data was filtered by wind (wind speeds greater than 2 m sec^{-1} and wind direction within the NNW–SSW sector), as well as by back-trajectory to exclude anomalies which were not associated with marine air masses. For the latter, trajectories could not reside for more than 36 hours of the total 120 hours over land, and could not travel more than 50 km inland past NDAO. A final data selection step was to exclude days that had

CO values greater than 15 ppb above baseline, to remove any time periods that may have been influenced by biomass burning. The filtered time series, with terrestrial influences removed, is shown in Figure 2.

2.3 Remote Sensing Data

Following the reasoning of Goubanova et al. (2013), sea surface temperature (SST) data were obtained from the Remote Sensing Systems (http://www.remss.com/) data archive. The Tropical Rainfall Measuring Mission (TRMM) Microwave Imager (TMI) daily optimally interpolated SST product was selected. The major advantage of this instrument is its ability to measure SST through clouds, which are considerable over the coast, as the TMI measures frequencies in the microwave region (4–11 GHz). The drawback of this dataset is that there is no data within 100 km of the coast. Large upwelling features, however, extend much farther out than this and are readily seen by TMI (Goubanova et al., 2013). Even with this loss of near-shore data, the data coverage is still superior to that of optical sensors like the Moderate-Resolution Imaging Spectroradiometer (MODIS). The TRMM SST data presented in this work is deseasonalized by subtracting a second harmonic fit to the data, as it showed a strong seasonal cycle which masked some of the intraseasonal variability when plotted as a time series.

Wind speed data for the South Atlantic was also derived from the TMI instrument on the TRMM satellite. This dataset is a level 3 product which gives the 10 m wind speed over marine areas within the sensor's field of view. The 18.7 GHz channel data product was selected. Like the SST data, a major drawback of this dataset is the absence of data within 100 km of land.

Two surface chlorophyll products were used, both level 3 binned products that combined data from multiple satellites, accessed through ESA GlobColour website (http://www.globcolour.info/). The first is denoted CHL1-GSM; this dataset is a merged product of two different sensors (during the time period considered), MODIS and the Visible Infrared Imaging Radiometer Suite (VIIRS). The data is merged using the Garver, Siegel, Maritorena (GSM) model, which blends the normalized water-leaving radiances instead of the end product (chl-a concentrations) (Maritorena and Siegel, 2005). The second product is denoted CHL1-AVW; these data are merged using a weighted average method (AVW). Like CHL1-GSM, it combines data from MODIS and VIIRS for the time frame considered.

2.4 Top-Down Air–Sea Flux Estimates

In order to estimate the surface flux associated with atmospheric anomalies due to upwelling events, the approach of Lueker et al. (2003) was adopted. A simple model was employed to describe the change in the concentration of a species within a well-mixed column of air as it moves over a source region (Jacob, 1999):

$$\Delta C = \begin{cases} \frac{F}{hq}\left(1 - e^{-\frac{qx}{U}}\right), & \text{for } 0 \le x \le L \\ \\ \Delta C_L\left(e^{-\frac{q(x-L)}{U}}\right), & \text{for } x \ge L \end{cases} \tag{3}$$

Here ΔC is the concentration of the species of interest, in mol m^{-3}, expressed as an anomaly against the background. ΔC is a function of x, which is the distance along a back-trajectory from NDAO to the area affected by upwelling. L is the point at which the column (with height h, in m) leaves this region, characterized by a constant flux, F, in mol m^{-2} hr^{-1}, and a constant wind speed, U, in m hr^{-1}. After the column leaves the flux region ($x \geq L$), the loss of ΔC from its peak at L (ΔC_L) is governed by dilution due to mixing of background air. This requires the dilution rate constant, q, in hr^{-1}, to be known.

Wind speeds (U) were obtained from satellite data (Section 2.3). h was taken as the average height of the planetary boundary layer (PBL) for the Lüderitz/Walvis Bay domain over the course of any given event. PBL data was acquired from the European Centre for Medium-Range Weather Forecasting's (ECMWF) ERA-Interim dataset (Dee et al., 1979). The dilution rate constant was estimated by comparing measurements of CO_2 and CH_4 made during the RV *Meteor* cruise M99 (see Section 2.5). Back-trajectories from NDAO were matched to the closest ship location at the appropriate time. Any back-trajectory points that were within 100 km of the ship—both horizontally and vertically—within the space of 1 hour were identified, and a dilution rate constant was calculated for both CO_2 and CH_4, as (Price et al., 2004):

$$q = \frac{1}{t} \ln \left(\frac{C_{M99} - C_b}{C_{NDAO} - C_b} \right) \tag{4}$$

Where C_{M99} and C_{NDAO} are the mole fractions of CO_2 or CH_4, as measured in situ on the *Meteor* or at NDAO, and C_b is taken from the fit to the baseline of the NDAO time series for either species, as described in Section 2.2. The values of q that were obtained from this exercise were then filtered to exclude for poor agreement between CO_2 and CH_4, and the average was taken to arrive at a single value, 0.011 ± 0.006 hr^{-1}.

2.5 In Situ Measurements During RV *Meteor* Cruise M99

Cruise M99 of the RV *Meteor* left Walvis Bay on July 31st, 2013, and returned to port on August 23rd. Continuous or semi-countinuous measurements of atmospheric CO_2, N_2O, and CH_4, as well as dissolved CO_2, O_2, and N_2O, were conducted throughout the cruise. Flask samples were taken for discreete measurements of $\delta(O_2/N_2)$.

Atmospheric measurements of CO_2 and CH_4 were made with a CRDS analyzer (model G1301, Picarro Inc, Santa Clara, CA, USA) located in the atmospheric chemistry laboratory. The instrument's internal pump was used to draw air through a 7 m length of 1/4" SERTOflex tubing, at a flow rate 150 mL min^{-1}. Inlets identical to those used at NDAO (Morgan et al., 2015) were placed on the starboard railing of the 6th superstructure deck, just above the atmospheric chemistry lab, at a total height of ~21 m above sea level. A second-order, instrument-specific water correction was performed in lieu of physical or chemical drying, identical to the method described in Morgan et al. (2015). As the instrument's pressure control seemed to be affected by strong vessel motion, measurements were excluded if the cavity pressure deviated by more than 0.04 torr. Calibrations were conducted on average every three days and target measurements were made once per day. Reference gases were calibrated at MPI-BGC GASLAB. The uncertainty, derived from the target measurements as at NDAO, was determined to be ± 0.03 ppm for CO_2 and ± 0.43 ppb for CH_4. The dataset was filtered for contamination by the ship's exhaust using the relative wind direction data from the ship's meteorological instrumentation.

Flasks for $\delta(O_2/N_2)$ were taken in triplicate and connected in series downstream of a pump. The pump body and valve plates were aluminum, and the structured diaphragms were made of PTFE. When in use the flow rate (3.2 L min^{-1}) was higher than the in situ analyzer flow rates (100–200 mL min^{-1}). Air was dried with a magnesium perchlorate. During sampling, the line was flushed for 5 minutes before any air was directed to the flasks, then a bypass valve was opened and the flasks were flushed for an additional 15 minutes before they were sealed again. After closure, the pressure of the flask was about 1.6 bars. Flasks were analyzed with a mass spectrometer at MPI-BGC (Brand, 2005). Storage times were less than two months.

Dissolved gas measurements were carried out by means of an autonomous setup for along-track measurements of CO_2, N_2O and CO, which combined the analytical approaches from Pierrot et al. (2009) and Arévalo-Martínez et al. (2013). A full description can be found in Arévalo-Martínez et al. (2019).

The estimated uncertainty of the dissolved CO_2 measurements was ± 2 μatm; of dissolved O_2 measurements, ± 4 μmol L^{-1}; of dissolved N_2O, ± 0.1 nmol L^{-1}. The uncertainty of the atmospheric measurements of N_2O was ± 0.9 ppb.

2.6 Shipboard Air–Sea Flux Density Estimates

In situ oceanographic and meteorological data were taken from the *Meteor*'s instrumentation. In order to determine the total dissolved inorganic carbon (DIC) content of surface waters, total alkalinity was estimated from temperature and salinity data, using the algorithm of Lee et al. (2006). The dissociation constants of carbonic acid were also determined from temperature and salinity using the formulations of Millero et al. (2006). The total DIC content was then estimated from the total alkalinity and $f\mathrm{CO}_2$. Meteorological data (air temperature, barometric pressure, wind speed, *etc.*) was observed at a height of 37 m above sea level. The absolute wind speed measured on the *Meteor* was converted to U_{10} through the relationship (Justus and Mikhail, 1976):

$$U_{10} = U_{meas}\left(\frac{z_{10}}{z_{meas}}\right)^{n} \tag{5}$$

$$n = \frac{0.37 - 0.0081 \cdot \ln(U_{meas})}{1 - 0.0881 \cdot \ln(\frac{z_{meas}}{10})} \tag{6}$$

where U_{meas} is the wind speed in m $\sec^{-1}$, measured at some height z_{meas}, in m.

Marine surface flux densities of CO_2, O_2, and N_2O were estimated for the vessel location throughout M99 from shipboard measurements of atmospheric dry air mole fractions and dissolved aqueous concentrations, according to Equation 7. While flux densities of CO were also determined, they are not discussed in this manuscript as the shipboard-measured flux was too small to be detected as an atmospheric anomaly at NDAO (contrary to what was reported in Morgan (2015)). In the case of O_2, the atmospheric concentration was measured only sporadically with flask samples, so it was taken as a static value, viz. the mole fraction of O_2 in standard dry air, 0.209392 (Tohjima et al., 2005). The in situ aqueous solubility of O_2 was calculated using the equations of García and Gordon (1992), of N_2O using those in Weiss and Price (1980), and of CO_2 using Weiss (1974). Sea-to-air fluxes (net evasion) are positive.

The flux density (F, in units of mol m^{-2} $\sec^{-1}$) is typically determined according to (Garbe et al., 2014):

$$F = k_w(C_w - \alpha C_a) \tag{7}$$

where k_w is the gas transfer (or piston) velocity, in m sec^{-1}, C_w is the dissolved concentration in the water phase (mol m^{-3}), and C_a is the concentration of the species in the air in the same units. The formulation can also be altered to accommodate units of partial pressure in both phases. The expression αC_a gives the dissolved concentration in the water phase directly at the surface; α is the Ostwald solubility coefficient: the reciprocal of the dimensionless air–water partition coefficient (K_{AW}) for some temperature, T, and salinity, S (Mackay and Shiu, 1981).

As there is no definitive k_w–U_{10} parameterization, fluxes were computed with three different parameterizations of k_w: that of Wanninkhof (1992) (k_{W92}), Nightingale et al. (2000) (k_{N00}), and McGillis et al. (2001) (k_{McG01}):

$$k_{\mathrm{W92}} = 0.31 U_{10}^2 \left(\frac{Sc}{660}\right)^{-0.5} \tag{8}$$

$$k_{\mathrm{N00}} = (0.222 U_{10}^2 + 0.333 U_{10}) \left(\frac{Sc}{600}\right)^{-0.5} \tag{9}$$

$$k_{\mathrm{McG01}} = (3.3 + 0.026 U_{10}^3) \left(\frac{Sc}{660}\right)^{-0.5} \tag{10}$$

In these equations, U_{10} is the wind speed at 10 m's height, and Sc is the Schmidt number of a particular gas at in situ conditions (Jähne et al., 1987; Wanninkhof, 1992). The Schmidt number is scaled to the reference conditions of the parameterization. The Schmidt number is dimensionless and k_w and U_{10} must be in the same units, *e.g.* m sec^{-1}; Schmidt numbers were calculated at in situ conditions by dividing the kinematic viscosity of seawater by the diffusivity of a given gas, using an Eyring-style equation (Eyring, 1936; Jähne et al., 1987):

$$D = A \exp\left(\frac{E_a}{RT}\right) \tag{11}$$

where R is the ideal gas constant, T is temperature, and E_a is the activation energy for diffusion in water. A and E_a are determined through fits to experimental data. For O_2 these were taken from Ferrell and Himmelblau (1967), for CO_2 from Jähne et al. (1987), and for N_2O from Bange et al. (2001). A salinity correction of 4.9% per 35.5 psu was then applied, this number being the average decrease in diffusivity seen by Jähne et al. (1987) for He and H_2 in an experiment involving artifical seawater. The kinematic viscosity of seawater at in situ conditions was determined by calculating the dynamic viscosity after Laliberté (2007) and the density after Millero and Huang (2009).

Note that the gas transfer velocity from Wanninkhof (1992) was included, even though it has since been revised (Wanninkhof, 2014), for purposes of comparability, since so many studies still make use of it.

3 Results and Discussion

3.1 Upwelling Events

In all, 173 days with upwelling events were identified, representing 24% of the two-year study period. From these 173, 102 had atmospheric conditions that allowed for the detection of an event. This was a conservative approach, since the filtering criteria in part relied on HYSPLIT model results, which could misrepresent the transport pathway and lead to the exclusion of an upwelling event that in fact was favorable for carrying an air mass influenced by upwelling to the station. Despite the greater prevalence of equatorward winds during austral summer, the distribution of events displayed little seasonality (Figure 3), reflecting the fact that upwelling is a short-term, intraseasonal phenomenon, forced by specific atmospheric conditions (Risien et al., 2004; Goubanova et al., 2013). While upwelling in this area is perennial, seasonality is seen in the intensity of upwelling due to the annual migration of the South Atlantic Anticyclone, with a minimum in austral winter (Hagen et al., 2001; Hardman-Mountford et al., 2003; Peard, 2007; Veitch et al., 2009; Hutchings et al., 2009).

An example of an upwelling event is given in Figures 1, 4, and 5. On November 27th, 2013, high winds resulted in the creation of a very large pool of colder water on the surface that persisted for four days, until winds relaxed and upwelling temporarily ceased until the 4th of December. During both upwelling events, chl-*a* values were higher. A change in the background values of atmospheric potential oxygen (APO), N_2O, and CH_4 was seen, with a smaller anomaly for CO_2. The largest anomalies for each species came when high winds were from the coastal sector on November 28th.

If the area of high flux was close to the coast, anomalies could arrive within a few hours at NDAO, with the development of the afternoon sea breeze. If the region of flux was closer to Lüderitz, the arrival time could be delayed by as much as 50 hours, depending on the wind speed and the degree of meandering of the air mass. Back-trajectories implied that despite the high wind speeds usually seen in this coastal zone, significant travel time (1 to 2 days) could be expected for most air masses of interest. As a result, the marine surface flux associated with an atmospheric anomaly could only be said to have taken place with 50 hours of its detection. The magnitudes of the average atmospheric anomalies and their corresponding flux density estimates are given in Table 1.

3.2 Estimated Top-Down Flux Densities

CO_2 fluxes were positive for all upwelling events, with an average flux density of 0.64 ± 0.4 μmol m^{-2} sec^{-1} and a maximum value of 1.6 μmol m^{-2} sec^{-1}. During upwelling conditions, it is not uncommon to see such strong outgassing of CO_2 in a coastal upwelling region; the biological response to new nutrients takes some days to draw down DIC levels (Torres et al., 1999; Loucaides et al., 2012; Cao et al., 2014). Santana-Casiano et al. (2009) used underway systems on cargo ships and weekly wind speeds to arrive at a mean flux between ca. -0.06 and 0.03 μmol m^{-2} sec^{-1} for the Lüderitz region, with peak rates as high as 0.06 μmol m^{-2} sec^{-1} in August. González-Dávila et al. (2009) found that the Lüderitz region is under-saturated with respect to CO_2, with only upwelled waters seeing oversaturation, with average fluxes on the order of -0.03 ± 0.3 μmol m^{-2} sec^{-1}. The flux densities for CO_2 reported in this study are not necessarily in conflict with these studies, since a yearly-averaged flux density is a different quantity from the event-based flux densities. The implication instead is that flux densities attributed to upwelling events are high enough to contribute significantly to the carbon balance of the Lüderitz and Walvis Bay regions.

Typical O_2 flux densities were about -5 μmol m^{-2} sec^{-1}. The O_2 flux densities inferred from APO are preferred over those calculated with atmospheric $\delta(O_2/N_2)$, as APO is explicitly formulated to remove land biosphere influences on the relative change in oxygen abundance. That the flux densities for O_2 calculated with these two formulations are so close is a good indication that the atmospheric data was primarily influenced by marine fluxes. These are high flux densities for the marine environment; the estimated average flux density for the entire mid-South Atlantic was $\sim$0.03 μmol m^{-2} sec^{-1} in the inverse modeling study of Gruber et al. (2001), and ca. 0.06 μmol m^{-2} sec^{-1} in the forward run of a coupled climate and ocean biogeochemistry model of Bopp et al. (2002).

The average flux density attributable to specific upwelling events for N_2O was 0.57 ± 0.3 nmol m^{-2} sec^{-1}, moderate for a coastal upwelling system. Surface data from the 2009 GENUS cruise would have yielded a maximum flux density of about 0.07–0.5 nmol m^{-2} sec^{-1}. Frame et al. (2014) observed flux rates as high as 0.52 nmol m^{-2} sec^{-1} in the Cape Frio upwelling cell. The 3-D coupled physical/biogeochemical model of Gutknecht et al. (2013b, a) predicts an 8-year mean flux density of 0.02–0.16 nmol m^{-2} sec^{-1} for the Walvis Bay region, including both shelf and deeper waters as far west as 10° E. The mean flux density of the entire M99 cruise was $\sim$0.03 nmol m^{-2} sec^{-1}. The model predicts a maximum flux density at the coast (22–24° S) of 0.6 nmol m^{-2} sec^{-1}. Arévalo-Martínez et al. (2019) reported considerably higher N_2O flux densities from a domain encompassing the latitude range of 16–28.5°S, ranging between 0.03 and 1.67 nmol m^{-2} sec^{-1}. For the Lüderitz/Walvis Bay area they found values similar to this study: up to 0.20 nmol m^{-2} sec^{-1}.

The moderate, positive CH_4 spikes ($\sim$10 ppb) seen during upwelling events corresponded to an average flux density of about 4 nmol m^{-2} sec^{-1} and a maximum of 33.5 nmol m^{-2} sec^{-1}, a high value even for coastal waters. There are few reported measurements of flux densities or dissolved CH_4 for the Benguela region to place these estimates in context. In what are likely the first measurements of dissolved methane in the Benguela, Scranton and Farrington (1977) observed concentrations near Walvis Bay at multiple depths in the 200–900 nM range. The only other available data known to the authors are from the 2009 GENUS cruise. These measurements were taken at a variety of depths (up to 400 m) and ranged from 4.7 to 140.0 nM. Using the three samples taken from the top 15 m from this cruise, at in situ conditions, a flux of 0.08–1.5 nmol m^{-2} sec^{-1} would be expected. Naqvi et al. (2010) used the data from Scranton and Farrington (1977) and from Monteiro et al. (2006) to estimate flux densities of 0.03–8.7 nmol m^{-2} sec^{-1}, the upper end-member of which compares favorably with the rates found in this study for the same ocean region. Though the latter study observed concentrations at a mooring near Walvis Bay as high as 10 μM, these data were from an uncalibrated probe and are not usable for a direct comparison to other campaigns. In other EBUS, reported flux densities are much lower.

3.3 M99: Atmospheric Measurements

Only CO_2 and CH_4 were measured continuously in the atmosphere on M99. During the first days of the cruise, a synoptic event brought elevated mixing ratios of CO_2 and CH_4 offshore (Figure 6). The shipboard measurements of CO_2 showed sporadic enhancements relative to the smoothed station background. This coincides with the regions of higher flux closer to the coast encountered under upwelling conditions (Figure 6 and 7). In contrast, CH_4 was consistently at background levels, usually below the value seen at NDAO.

3.4 M99: Dissolved Gas Concentrations

All three species measured underway in the water phase showed the largest deviation from atmospheric equilibrium closest to shore (Figure 7). $f\mathrm{CO_2}$ ranged from 355.5 to 852.3 μatm (87.8% to 207.3% saturation), with most of the observed oversaturation occurring under upwelling conditions. Dissolved oxygen was mostly at saturation or slightly above, although close to shore the concentration dropped to a minimum of 180.8 μM (67% saturation). N_2O surface concentrations were rather low for an upwelling region, but agreed well with previously reported values, with the maximum observed concentration of 20.5 nM being comparable to the highest values seen by Frame et al. (2014) for surface measurements in the same region. Recently, Arévalo-Martínez et al. (2019) reported surface N_2O concentrations ranging between 8 and 31 nM for the northern Benguela region. Besides this, the only other in situ measurements of N_2O in the Benguela region known to the authors are in the Marine Methane and Nitrous Oxide (MEMENTO; https://memento.geomar.de/de) database (Bange et al., 2009; Kock and Bange, 2015), from a single cruise in 2009 aboard the FRS *Africana*. In this dataset, dissolved N_2O concentrations for surface waters (the top 15 m) were in the range of 5–51 nM, which brackets the range measured during M99.

The main upwelling event of the cruise, in the Lüderitz/Walvis Bay cell, began on August 4th, 2013, and lasted until August 11th (Figure 8). Wind speeds declined rapidly after the 8th. The upwelling event was encountered by the *Meteor* starting on the 8th, as the vessel reached an upwelling filament, the outer edge of which was subject to net evasion of all three gases (CO_2, O_2, N_2O), likely a result of warming temperatures that would reduce their solubility.

3.5 Comparison of Top-Down and Bottom-Up Flux Density Estimates

Due to local wind variability, suitable conditions for detecting the upwelling event encountered by the *Meteor* were only seen at NDAO on the 6th, 8th, and 10th of August, 2013. As the vessel was not always in the upwelling cell, only a single atmospheric anomaly at NDAO could be matched to in situ shipboard measurements, namely an anomaly occurring on August 10th. The top-down estimates agreed reasonably with the corresponding mean shipboard estimates for a selected 7.5 hour period that coincided with the largest flux densities (Figure 8 and Table 2). The highest flux rates (positive for CO_2 and N_2O, and negative for O_2) were seen within the recently upwelled waters experiencing high wind speeds. Fluxes displayed coupling between all three species, though the area of high flux density for O_2 and N_2O was more sharply defined than for CO_2.

The choice of gas transfer velocity parameterization was significant in determining the magnitude of the agreement, and the degree of this correspondence between the top-down and shipboard gas transfer velocity-specific estimate varied between species. For CO_2 the choice of the gas transfer velocity parameterization (k_w) was, in order of descending agreement: $\mathrm{k_{W92}}$, $\mathrm{k_{McG01}}$, and $\mathrm{k_{N00}}$; for O_2 and N_2O, $\mathrm{k_{McG01}}$, $\mathrm{k_{W92}}$, $\mathrm{k_{N00}}$. While this provides a measure of confidence in the top-down flux density estimates, it should be noted that the neither of the estimated uncertainties for the top-down or bottom-up approaches account for errors incurred by the simplifying assumptions within their formulations, and these comparisons should not be considered a “calibration” of the flux determination or k_w parameterization.

Biogeosciences Discuss., https://doi.org/10.5194/bg-2019-103
Manuscript under review for journal Biogeosciences
Discussion started: 26 March 2019

3.6 Stoichiometry

Correlation slopes of atmospheric species can provide further confidence and insight into source processes, if there is an underlying biogeochemical relationship. The well-known inverse relationship between N_2O and O_2 in the ocean, for instance, is a result of organic matter decomposition and nitrification (Cohen and Gordon, 1979; Nevison et al., 2003; Naqvi et al., 2010; Frame et al., 2014). The tight coupling between N_2O and O_2 seen in surface concentrations during M99 is preserved during air–sea gas exchange, as these gases behave similarly (Figure 9). The observed linear correlation in surface waters between these two species is also an indication that intense denitrification was not occurring in the OMZ at the time of sampling, which if it were taking place, would lead to a breakdown in this relationship at low O_2 (Cohen and Gordon, 1979). The approximate molar ratio of these two species, -0.8×10^{-4} to -1×10^{-4} (N_2O:O_2; mol mol^{-1}), is the same observed by Lueker et al. (2003) for the Trinidad Head region, and appears to be a globally consistent value (Nevison et al., 2005; Manizza et al., 2012).

This linear regression slope is often expressed in terms of the excess N_2O (measured N_2O minus N_2O at saturation) and apparent oxygen utilization (saturation minus observed), ΔN_2O–AOU in nmol μmol^{-1}. Quantified in this way, it has been used as an estimate of the yield of N_2O as a function of the amount of oxygen consumed (Nevison et al., 2003). However, the relationship is not strictly linear, since N_2O production is enhanced at low oxygen levels (Nevison et al., 2003; Naqvi et al., 2010; Trimmer et al., 2016). ΔN_2O–AOU is also sensitive to mixing, as N_2O production rates vary widely in the ocean, meaning that the mixing of water masses with different compositions can overwhelm the in situ production signal (Suntharalingam and Sarmiento, 2000; Nevison et al., 2003). The ΔN_2O–AOU for M99 was 0.088 ± 0.003 nmol μmol^{-1}, with an intercept of 1.6 ± 0.04 nmol, and an R^2 of 0.69. This is a low value, nearly identical to results from the eastern basin of the sub-tropical North Atlantic, where South Atlantic Central Water is found (Cohen and Gordon, 1979; Suntharalingam and Sarmiento, 2000; Walter et al., 2006), and the eastern equatorial Atlantic (Arévalo-Martínez et al., 2017). Frame et al. (2014) showed that most of the N_2O in the Benguela Current region is produced in the water column and in the sediment by nitrifier denitrification (Frame et al., 2014). Nevertheless, a substantial portion of this N_2O remains at depth (with a concentration maximum at 200–400 m) and is advected away from the region, without the chance for atmospheric release (Gutknecht et al., 2013b, a; Frame et al., 2014). Hence, the low ΔN_2O–AOU value found for the *Meteor* cruise probably reflects both physical and biogeochemical dynamics.

In the case of variations of O_2 and CO_2, the stoichiometry of surface waters is not preserved after air–sea exchange, as the majority of carbon is speciated in the carbonate system, and only the portion that remains as dissolved CO_2 is available for air–sea gas exchange. This leads to a change in the ratio, for instance, from 0.58 ± 0.03 in surface waters to -6.53 ± 0.42 in the atmosphere, for the upwelling event encountered during the R/V *Meteor* cruise M99 (Figure 8). These two species can become decoupled through the influences of changing solubility, which would drive evasion of both gases, and net biological production, which would drive evasion of O_2 and invasion of CO_2. These complicating influences are the likely reason for the poorer correlation seen between these two species when compared with N_2O and O_2.

While the top-down flux density estimates cannot be confirmed with shipboard estimates of flux densities for CH_4, it is worth considering that concentrations of methane in bottom waters on the Namibian shelf are likely the highest ever measured in an open coastal system. Values as high as 475 μM in the bottom waters and greater than 5,000 μM in sediment porewaters have been observed (Scranton and Farrington, 1977; Monteiro et al., 2006; Brüchert et al., 2009; Naqvi et al., 2010). In the water column, the concentration maxima is usually at the seabed or in bottom water, but it is variable and can even occur at the surface (1 m) (Brüchert et al., 2009). Dissolved methane concentrations are tightly coupled with O_2 and show considerable variability, with elevated concentrations being triggered by episodes of hypoxia (Monteiro et al., 2006; Brüchert et al., 2009). The pulse-like nature of CH_4 in the Benguela means that the full range of dynamics cannot be captured with a campaign-based sampling approach (Brüchert et al., 2009). What is clear is that there is a tremendous amount of methane production at depth, but that the source is variable in strength (Emeis et al., 2004; Brüchert et al., 2009). In light of the fact that large pockets of free methane gas are contained in the sediment in the Walvis Bay region, as well as the existence of craters and pockmarks on the seafloor, combined with observation of bubble streams from the seabed, suggest a mechanism by which methane produced in sediments can be abruptly transported to the surface and hence, avoid oxidation (Emeis et al., 2004; Brüchert et al., 2006, 2009). Consequently, the Benguela Current is a suspected source of CH_4 to the atmosphere, but the amount is ill-constrained (Naqvi et al., 2010); Emeis et al. (2013) recently estimated the total annual emission for the entire system to be less than 0.17 Tg CH_4 yr^{-1}.

Interestingly, methane was not well-correlated with either APO or CO_2 in the atmosphere during all upwelling events, suggesting a spatial decoupling (since a cross-correlation analysis indicated this was not a result of lag/temporal decoupling) between methane and these two species. While background observations of CH_4 were generally well-correlated with CO_2 and O_2 at NDAO, only some upwelling events showed such coupling; it seems there is a general relationship between methane and oxygen, but it is not consistent and is occasionally non-existent. Unfortunately, since there are still very few measurements of water-column CH_4 in the Benguela, a full explanation of the methane source remains elusive. From these atmospheric trends it can only be deduced that there is some separate biogeochemical influence on methane that is not exerted over CO_2, O_2, or N_2O. This observation is arguably consistent with the concept of a dominant sedimentary source of methane that is more localized within the inshore mud belt, where high POC fluxes have created a thick layer of diatomaceous ooze containing free methane gas pockets (Emeis et al., 2004; Brüchert et al., 2006; van der Plas et al., 2007; Brüchert et al., 2009).

4 Summary and Conclusions

We have shown that coastal atmospheric anomalies of CO_2, O_2, N_2O, and CH_4 can be related to upwelling events in the Lüderitz and Walvis Bay cells. Using a simple model, we have estimated the flux density of the four species relating to upwelling events. These top-down estimates of surface fluxes have been found to be in good agreement with in situ surface flux densities as determined from shipboard measurements. Our study highlights the usefulness of continuous monitoring in order to achieve a more accurate estimation of the emissions of GHGs from coastal upwelling systems, since the large impact of small temporal and spatial scales of variability are prone to be overlooked by in-situ surveys.

The Lüderitz and Walvis Bay upwelling cells have been shown to be potentially an unusually large source of CH_4 to the atmosphere for the marine environment. In contrast, the region is a weaker source of N_2O, compared to other upwelling regions, a fact which has been predicted from modeling studies and noted in observations of dissolved concentrations and air–sea fluxes. This upwelling area also functions as a significant source term in the CO_2 budget of the Benguela Current. Based on our results and previous studies (Nevison et al., 2004; Lueker et al., 2003) we suggest to establish a network of high-resolution atmospheric GHG measurements adjacent to major coastal upwelling regions in order to monitor their GHG emissions. Continuous land-based monitoring will help to establish time series of coastal GHG fluxes which are needed to account for the seasonal variability and to detect both short-term and long-term trends of coastal GHG emissions.

Data availability. The atmospheric data from NDAO is included as part of the Supporting Information. M99 N_2O and CO_2 data will be uploaded to the MarinE MethanE and NiTrous Oxide database (MEMENTO, https://memento.geomar.de/) and the Surface Ocean CO_2 Atlas (SOCAT, https://www.socat.info/), respectively, after publication.

Author contributions. M.H. and J.L. conceived of the location and motivation for the atmospheric observatory. E.J.M., J.L., and T. Seifert conducted the atmospheric observations in Namibia of all species and on the RV *Meteor* for CO_2, CH_4, and $\delta(O_2/N_2)$. D.L.A.-M. and T. Steinhoff made the underway measurements of the other dissolved and atmospheric gases on the *Meteor*. E.J.M. wrote the manuscript, and all authors made substantial contributions to the text and/or analyses.

Competing interests. The authors declare that they have no conflict of interest.

Acknowledgements. The authors wish to express their gratitude to the Master, crew, and Chief Scientist (Detlef Quadfasel) of the RV *Meteor* during leg M99, and to the government of Namibia for permission to work in Namibian territorial waters. This work is a contribution to SOPRAN III (BMBF grant# FKZ 03F0662). SATRE collaborators Gregor Rehder and Jan Werner (Leibniz Institute for Baltic Sea Research) operated the $N_2O/CO/CO_2$ underway system throughout the cruise. Tim Rixen (Leibniz Center for Tropical Marine Ecology/University of Hamburg) kindly provided the GENUS cruise data, as well as helpful comments on this manuscript. We also thank and acknowledge Gillian Maggs-Kölling, Theo Wassenaar, Jessica Sack, Tayler Chicoine, Robert Logan, and the Gobabeb community for their technical support and hospitality. The authors are grateful for the efforts and expertise of Armin Jordan, Willi Brand, Michael Hielscher, Bert Steinberg, Johannes Schwarz, and Jürgen Richter (MPI-BGC) in preparing and analyzing flask samples and gas cylinders. Author D.L.A.M. was supported by the EU FP7 project InGOS (Grant Agreement #284274). Author E.J.M. was a part of the International Max Planck Research School for Global Biogeochemical Cycles when this work was conducted and acknowledges its funding and support. Funding for the research activities presented here was provided by the Max Planck Society.

References

Amante, C. and Eakins, B.: ETOPO1 1 Arc-Minute Global Relief Model: Procedures, Data Sources and Analysis. NOAA Technical Memorandum NESDIS NGDC-24. National Geophysical Data Center, NOAA. DOI:10.7289/V5C8276M, 2009.

Arévalo-Martínez, D., Kock, A., Steinhoff, T., Brandt, P., Dengler, M., Fischer, T., Körtzinger, A., and Bange, H. W.: Nitrous oxide during the onset of the Atlantic cold tongue, Journal of Geophysical Research: Oceans, 122, 171–184, https://doi.org/10.1002/2016JC012238, 2017.

Arévalo-Martínez, D. L., Beyer, M., Krumbholz, M., Piller, I., Kock, A., Steinhoff, T., Körtzinger, A., and Bange, H. W.: A new method for continuous measurements of oceanic and atmospheric N_2O, CO and CO_2: performance of off-axis integrated cavity output spectroscopy (OA-ICOS) coupled to non-dispersive infrared detection (NDIR), Ocean Science, 9, 1071–1087, https://doi.org/10.5194/os-9-1071-2013, 2013.

Arévalo-Martínez, D. L., Kock, A., Löscher, C. R., Schmitz, R. A., and Bange, H.: Massive nitrous oxide emissions from the tropical South Pacific Ocean, Nature Geoscience, 8, 530–533, 2015.

Arévalo-Martínez, D. L., Steinhoff, T., Brandt, P., Körtzinger, A., Lamont, T., Rehder, G., and Bange, H. W.: N_2O emissions from the northern Benguela upwelling system, Geophysical Research Letters, https://doi.org/10.1029/2018GL081648, 2019.

Babbin, A., Bianchi, D., Jayakumar, A., and Ward, B.: Rapid nitrous oxide cycling in the suboxic ocean, Science, 348, 1127–1130, 2015.

Bange, H., Andreae, M., Lal, S., Law, C., Naqvi, S., Patra, P., Rixen, T., and Upstill-Goddard, R.: Nitrous oxide emissions from the Arabian Sea: A synthesis, Atmospheric Chemistry and Physics, 1, 61–71, https://doi.org/10.5194/acp-1-61-2001, 2001.

Bange, H., Bell, T., Cornejo, M., Freing, A., Uher, G., Upstill-Goddard, R., and Zhang, G.: MEMENTO: a proposal to develop a database of marine nitrous oxide and methane measurements, Environmental Chemistry, 6, 195–197, https://doi.org/10.1071/EN09033, 2009.

Bianchi, D., Dunne, J., Sarmiento, J., and Galbraith, E.: Data-based estimates of suboxia, denitrification, and N_2O production in the ocean and their sensitivities to dissolved O_2, Global Biogeochemical Cycles, 26, GB2009, 2012.

Blanke, B., Speich, S., Bentamy, A., Roy, C., and Sow, B.: Modeling the structure and variability of the southern Benguela upwelling using QuikSCAT wind forcing, Journal of Geophysical Research: Oceans, 110, C07 018, https://doi.org/10.1029/2004JC002529, 2005.

Bopp, L., Le Quéré, C., Heimann, M., Manning, A., and Monfray, P.: Strong CO_2 emissions from the Arabian Sea during South-West Monsoon, Global Biogeochemical Cycles, 16, 1022, https://doi.org/10.1029/2001GB001445, 2002.

Brand, W.: O_2/N_2 Storage Aspects and Open Split Mass Spectrometric Determination, in: Proceedings of the 12^{th} WMO/IAEA Meeting of Experts on Carbon Dioxide, Other Greenhouse Gases and Related Tracers Measurement Techniques, WMO/TD-No. 1275, edited by Worthy, D. and Huang, L., WMO, Geneva, Switzerland, 2005.

Brüchert, V., Currie, B., Peard, K., Lass, U., Endler, R., Dübecke, A., Julies, E., Leipe, T., and Zitzmann, S.: Biogeochemical and Physical Control on Shelf Anoxia and Water Column Hydrogen Sulphide in the Benguela Coastal Upwelling System Off Namibia, in: *Past and Present Water Column Anoxia*, edited by Neretin, L., pp. 161–193, Springer, the Netherlands, 2006.

Brüchert, V., Currie, B., and Peard, K.: Hydrogen sulphide and methane emissions on the central Namibian shelf, Progress in Oceanography, 83, 169–179, 2009.

Cao, Z., Dai, M., Evans, W., Gan, J., and Feely, R.: Diagnosing CO_2 fluxes in the upwelling system off the Oregon–California coast, Biogeosciences, 11, 6341–6354, https://doi.org/10.5194/bg-11-6341-2014, 2014.

Capone, D. and Hutchins, D.: Microbial biogeochemistry of coastal upwelling regimes in a changing ocean, Nature Geoscience, 6, 711–717, https://doi.org/10.1038/ngeo1916, 2013.

Cohen, Y. and Gordon, L.: Nitrous Oxide Production in the Ocean, Journal of Geophysical Research, 84, 347–353, 1979.

Cornejo, M., Farías, L., and Paulmier, A.: Temporal variability in N_2O water content and its air–sea exchange in an upwelling area off central Chile (36° S), Marine Chemistry, 101, 85–94, 2006.

Dee, D., Uppala, S., Simmons, A., Berrisfold, P., Poli, P., Kobayashi, S., Andrea, U., Balmaseda, A., Balsamo, G., Bauer, P., Bechtold, P., Beljaars, A., van de Berg, L., Bidlot, J., Bormann, N., Delsol, C., Dragani, R., Fuentes, M., Geer, A., Haimberger, L., Healy, S., Hersbach, H., Hólm, E., Isaksen, L., Kållberg, P., Köhler, M., Matricardi, M., McNally, A., Monge-Sanz, B., Morcrette, J.-J., Park, B.-K., Peubey, C., de Rosnay, P., Tavolato, C., Thépaut, J.-N., and Vitart, F.: The ERA-Interim reanalysis: configuration and performance of the data assimilation system, Quarterly Journal of the Royal Meteorlogical Society, 137, 553–597, 1979.

Demarcq, H., Barlow, R., and Hutchings, L.: Application of a chlorophyll index derived from satellite data to investigate the variability of phytoplankton in the Benguela system, African Journal of Marine Science, 29, 271–282, 2007.

Desbiolles, F., Blanke, B., and Bentamy, A.: Short-term upwelling events at the western African coast related to synoptic atmospheric structures as derived from satellite observations, Journal of Geophysical Research: Oceans, 119, 1–23, https://doi.org/10.1002/2013JC009278, 2014a.

Desbiolles, F., Blanke, B., Bentamy, A., and Grima, N.: Origin of fine-scale wind stress curl structures in the Benguela and Canary upwelling systems, Journal of Geophysical Research: Oceans, 119, 7931–7948, https://doi.org/10.1002/2014JC010015, 2014b.

Emeis, K., Anja, E., Anita, F., Niko, L., Günther, N., Andreas, N., Rixen, T., Schmidt, M., Van der Plas, A., and Norbert, W.: Biogeochemical processs and turnover rates in the Northern Benguela Upwelling System, Journal of Marine Systems, 6, 63–80, https://doi.org/10.1038/ngeo1916, 2013.

Emeis, K.-C., Brüchert, V., Currie, B., Endler, R., Ferdelman, T., Kiessling, A., Leipe, T., Noli-Peard, K., Struck, U., and Vogt, T.: Shallow gas in shelf sediments of the Namibian coastal upwelling ecosystem, Continental Shelf Research, 24, 627–642, 2004.

Evans, W., Hales, B., and Strutton, P.: Seasonal cycle of surface ocean $p\mathrm{CO}_2$ on the Oregon shelf, Journal of Geophysical Research, 116, C05 012, https://doi.org/10.1029/2010JC006625, 2011.

Evans, W., Hales, B., Strutton, P., Shearman, R., and Barth, J.: Failure to bloom: Intense upwelling results in negligible phytoplankton response and prolonged CO_2 outgassing over the Oregon shelf, Journal of Geophysical Research: Oceans, 120, https://doi.org/10.1002/2014JC010580, 2015.

Eyring, H.: Viscosity, Plasticity, and Diffusion as Examples of Absolute Reaction Rates, Journal of Chemical Physics, 4, 283–291, 1936.

Ferrell, R. and Himmelblau, D.: Diffusion Coefficients of Nitrogen and Oxygen in Water, Journal of Chemical and Engineering Data, 12, 111–115, 1967.

Frame, C., Deal, E., Nevison, C., and Casciotti, K.: N_2O production in the eastern South Atlantic: Analysis of N_2O stable isotopic and concentration data, Global Biogeochemical Cycles, 28, https://doi.org/10.1002/2013GB004790, 2014.

Garbe, C., Rutgersson, A., Boutin, J., de Leeuw, G., Delille, B., Fairall, C., Gruber, N., Hare, J., Ho, D., Johnson, M., Nightingale, P., Pettersson, H., Piskozub, J., Sahlée, E., Tsai, W.-T., Ward, B., Woolf, D., and Zappa, C.: Transfer Across the Air–Sea Interface, in: *Ocean-Atmosphere Interactions of Gases and Particles*, edited by Liss, P. and Johnson, M., pp. 55–112, Springer, Heidelberg, Germany, 2014.

García, H. and Gordon, L.: Oxygen solubility in seawater: Better fitting equations, Limnology and Oceanography, 37, 1307–1312, 1992.

González-Dávila, M., Santana-Casiano, J., and Ucha, I.: Seasonal variability of $f\mathrm{CO}_2$ in the Angola-Benguela region, Progress in Oceanography, 83, 124–133, 2009.

Goubanova, K., Illig, S., Machu, E., Garçon, V., and Dewitte, B.: SST subseasonal variability in the central Benguela upwelling system as inferred from satellite observations (1999–2009), Journal of Geophysical Research: Oceans, 118, https://doi.org/10.1002/jgrc.20287, 2013.

Gregor, L. and Monteiro, P.: Is the southern Benguela a significant regional sink of CO_2?, South African Journal of Science, 109, 0094, https://doi.org/10.1590/sajs.2013/20120094, 2013.

Gruber, N., Gloor, M., Fan, S.-M., and Sarmiento, J.: Air-sea flux of oxygen estimated from bulk data: Implications for the marine and atmospheric oxygen cycles, Global Biogeochemical Cycles, 15, 783–803, 2001.

Gutknecht, E., Dadou, I., Le Vu, B., Cambon, G., Sudre, J., Garçon, V., Machu, E., Rixen, T., Kock, A., Flohr, A., Paulmier, A., and Lavik, G.: Coupled physical/biogeochemical modeling including O_2-dependent processes in the Eastern Boundary Upwelling Systems: application in the Benguela, Biogeosciences, 10, 3559–3591, https://doi.org/10.5194/bg-10-3559-2013, 2013a.

Gutknecht, E., Dadou, I., Marchesiello, P., Cambon, G., Le Vu, B., Sudre, J., Garçon, V., Machu, E., Rixen, T., Kock, A., Flohr, A., Paulmier, A., and Lavik, G.: Nitrogen transfers off Walvis Bay: a 3-D coupled physical/biogeochemical modeling approach in the Namibian upwelling system, Biogeosciences, 10, 4117–4135, https://doi.org/10.5194/bg-10-4117-2013, 2013b.

Hagen, E., Feistel, R., Agenbag, J., and Ohde, T.: Seasonal and interannual changes in Intense Benguela Upwelling (1982–1999), Oceanologica Acta, 24, 557–568, 2001.

Hardman-Mountford, N., Richardson, A., Agenbag, J., Hagen, E., Nykjaer, L., Shillington, F., and Villacastin, C.: Ocean climate of the South East Atlantic observed from satellite data and wind models, Progress in Oceanography, 59, 181–221, 2003.

Hutchings, L., van der Lingen, C., Shannon, L., Crawford, R., Verheye, H., Bartholomae, C., van der Plas, A., Louw, D., Kreiner, A., Ostrowski, M., Fidel, Q., Barlow, R. G., Lamont, T., Coetzee, J., Shillington, F., Veitch, J., Currie, J. C., and Monteiro, P.: The Benguela Current: An ecosystem of four components, Progress in Oceanography, 83, 15–32, 2009.

Jacob, D.: Introduction to Atmospheric Chemistry, Princeton University Press, Princeton, NJ, 1999.

Jähne, B., Heinz, G., and Dietrich, W.: Measurement of the Diffusion Coefficients of Sparingly Soluble Gases in Water, Journal of Geophysical Research, 92, 10,767–10,776, 1987.

Justus, C. and Mikhail, A.: Height variation of wind speed and wind distributions statistics, Geophysical Research Letters, 3, 261–264, 1976.

Keeling, R. and Shertz, S.: Seasonal and interannual variations in atmospheric oxygen and implications for the global carbon cycle, Nature, 358, 723–727, 1992.

Kock, A. and Bange, H. W.: Counting the Ocean's Greenhouse Gas Emissions, Eos, 96, 10–13, https://doi.org/10.1029/2015eo023665, 2015.

Laliberté, M.: Model for Calculating the Viscosity of Aqueous Solutions, Journal of Chemical and Engineering Data, 52, 321–335, 2007.

Laruelle, G., Lauerwald, R., Pfeil, B., and Regnier, P.: Regionalized global budget of the CO_2 exchange at the air-water interface in continental shelf seas, Geophysical Research Letters, 28, 1199–1214, https://doi.org/10.1002/2014GB004832, 2014.

Lee, K., Tong, L., Millero, F., Sabine, C., Dickson, A., Goyet, C., Park, G.-H., Wanninkhof, R., Feely, R., and Key, R.: Global relationships of total alkalinity with salinity and temperature in surface waters of the world's oceans, Geophysical Research Letters, 33, L19 605, https://doi.org/10.1029/2006GL027207, 2006.

Levin, L., Liu, K., Emeis, K.-C., Breitburg, D., Cloern, J., Deutsch, C., Giani, M., Goffart, A., Hofmann, E., Lachkar, Z., Limburg, K., Liu, S.-M., Montes, E., Naqvi, W., Ragueneau, O., Rabouille, C., Sarkar, S., Swaney, D., Wassman, P., and Wishner, K.: Comparative biogeochemistry–ecosystem–human interactions on dynamic continental margins, Journal of Marine Systems, 141, 3–17, https://doi.org/10.1016/j.jmarsys.2014.04.016, 2015.

Loucaides, S., Tyrrell, T., Achterberg, E., Torres, R., Nightingale, P., Kitidis, V., Serret, P., Woodward, M., and Robinson, C.: Biological and physical forcing of carbonate chemistry in an upwelling filament off northwest Africa: Results from a Lagrangian study, Global Biogeochemical Cycles, 26, GB3008, https://doi.org/10.1029/2011GB004216, 2012.

Lueker, T.: Coastal upwelling fluxes of O_2, N_2O, and CO_2 assessed from continuous atmospheric observations at Trinidad, California, Biogeosciences, 1, 101–111, 2004.

Lueker, T., Walker, S., Vollmer, M., Keeling, R., Nevison, C., and Weiss, R.: Coastal Upwelling air-sea fluxes revealed in atmospheric observations of O_2/N_2, CO_2 and N_2O, Geophysical Research Letters, 30, 1292, 2003.

Lutjeharms, J. and Meeuwis, J.: The extent and variability of South-East Atlantic upwelling, South African Journal of Marine Science, 5, 51–62, 1987.

Mackay, D. and Shiu, W.: A Critical Review of Henry's Law Constants for Chemicals of Environmental Interest, Journal of Physical and Chemical Reference Data, 10, 1175–1199, 1981.

Manizza, M., Keeling, R., and Nevsion, C.: On the processes controlling the seasonal cycles of the air–sea fluxes of O_2 and N_2O: A modelling study, Tellus B, 64, 18 429, https://doi.org/10.3402/tellusb.v64i0.18429, 2012.

Maritorena, S. and Siegel, D.: Consistent merging of satellite ocean color data sets using a bio-optical model, Remote Sensing of Environment, 94, 429–440, 2005.

McGillis, W., Edson, J., Ware, J., Dacey, J., Hare, J., Fairall, C., and Wanninkhof, R.: Carbon dioxide flux techniques performed during GasEx-98, Marine Chemistry, 75, 267–280, 2001.

Millero, F. and Huang, F.: The density of seawater as a function of salinity (5 to 70 g kg^{-1}) and temperature (273.15 to 363.15 K, Ocean Science, 5, 91–100, 2009.

Millero, F., Graham, T., Huang, F., Bustos-Serrano, H., and Pierrot, D.: Dissociation constants of carbonic acid in seawater as a function of salinity and temperature, Marine Chemistry, 100, 80–94, https://doi.org/10.1016/j.marchem.2005.12.001, 2006.

Monteiro, P., van der Plas, A., Mohrholz, V., Mabille, E., Pascall, A., and Joubert, W.: Variability of natural hypoxia and methane in a coastal upwelling system: Oceanic physics or shelf biology?, Geophysical Research Letters, 33, L16 614, 2006.

Morgan, E.: Continuous Measurements of Greenhouse Gases and Atmospheric Oxygen in the Namib Desert, Ph.D. thesis, Christian-Albrechts-Universität zu Kiel, 2015.

Morgan, E., Lavrič, J., Seifert, T., Chicoine, T., Day, A., Gomez, J., Logan, R., Sack, J., Shuuya, T., Uushona, E., Vincent, K., Schultz, U., Brunke, E.-G., Labuschagne, C., Thompson, R., Schmidt, S., Manning, A., and Heimann, M.: Continuous measurements of greenhouse gases and atmospheric oxygen at the Namib Desert Atmospheric Observatory, Atmospheric Measurement Techniques, 8, 2233–2250, https://doi.org/10.5194/amt-8-2233-2015, 2015.

Naqvi, S., Bange, H., Farías, L., Monteiro, P., Scranton, M., and Zhang, J.: Marine hypoxia/anoxia as a source of CH_4 and N_2O, Biogeosciences, 7, 2159–2190, https://doi.org/10.5194/bg-7-2159-2010, 2010.

Nevison, C., Butler, J., and Elkins, J.: Global distribution of N_2O and the ΔN_2O-AOU yield in the subsurface ocean, Global Biogeochemical Cycles, 17, 1119, 2003.

Nevison, C., Lueker, T., and Weiss, R.: Quantifying the nitrous oxide source from coastal upwelling, Global Biogeochemical Cycles, 18, GB1018, https://doi.org/10.1029/2003GB002110, 2004.

Nevison, C., Keeling, R., Weiss, R., Popp, B., Jin, X., Fraser, P., Porter, L., and Hess, P.: Southern Ocean ventilation inferred from seasonal cycles of atmospheric N_2O and O_2/N_2 at Cape Grim, Tasmania, Tellus, 57B, 218–229, 2005.

Nightingale, P., Malin, G., Law, C., Watson, A., Liss, P., Liddicoat, M., Boutin, J., and Upstill-Goddard, R.: In situ evaluation of air-sea gas exchange parameterizations using novel conservative volatile tracers, Global Biogeochemical Cycles, 14, 373–387, 2000.

Peard, K.: Seasonal and Interannual Variability of Wind-Driven Upwelling at Lüderitz, Namibia, Master's thesis, University of Cape Town, 2007.

Pierrot, D., Neill, C., Sullivan, K., Castle, R., Wanninkhof, R., Lüger, H., Johannessen, T., Olsen, A., Feely, R., and Cosca, C.: Recommendations for autonomous underway $p\mathrm{CO}_2$ measuring systems and data-reduction routines, Deep-Sea Research II, 56, 512–522, https://doi.org/10.1016/j.dsr2.2008.12.005, 2009.

Price, H., Jaffe, D., Cooper, O., and Doskey, P.: Photochemistry, ozone production, and dilution during long-range transport episodes from Eurasia to the northwest United States, Journal of Geophysical Research, 109, D23S13, 2004.

Rehder, G., Collier, R., Heeschen, K., Kosro, P., Barth, J., and Suess, E.: Enhanced marine CH_4 emissions to the atmosphere off Oregon caused by coastal upwelling, Global Biogeochemical Cycles, 16, 1081, https://doi.org/10.1029/2000GB001391, 2002.

Reimer, J., Vargas, R., Smith, S., Lara-Lara, R., Gaxiola-Castro, G., Hernández-Ayón, J., Castro, A., Escoto-Rodriguez, M., and Martínez-Osuna, J.: Air–sea CO_2 fluxes in the near-shore and intertidal zones influenced by the California Current, Journal of Geophysical Research: Oceans, 118, 1–16, 2013.

Risien, C., Reason, C., Shillington, F., and Chelton, D.: Variability in satellite winds over the Benguela upwelling system during 1999–2000, Journal of Geophysical Research, 109, C03 010, 2004.

Rödenbeck, C., Quéré, L., Heimann, M., and Keeling, R.: Interannual variability in oceanic biogeochemical processes inferred by inversion of atmospheric O_2/N_2 and CO_2 data, Tellus, 60B, 685–705, 2008.

Sansone, F., Popp, B., Gasc, A., Graham, A., and Rust, T.: Highly elevated methane in the eastern tropical North Pacific and associated isotopically enriched fluxes to the atmosphere, Geophysical Research Letters, 28, 4567–4570, https://doi.org/10.1029/2001GL013460, 2001.

Santana-Casiano, J., González-Dávila, M., and Ucha, I.: Carbon dioxide fluxes in the Benguela upwelling system during winter and spring: A comparison between 2005 and 2006, Deep-Sea Research II, 56, 533–541, 2009.

Scranton, M. and Farrington, J.: Methane Production in the Waters off Walvis Bay, Journal of Geophysical Research, 82, 4947–4953, 1977.

Severinghaus, J.: Studies of the terrestrial O_2 and carbon cycles in sand dune gases and in Biosphere 2, Ph.D. thesis, Columbia University, 1995.

Stephens, B., Keeling, R., Heimann, M., Six, K., Murnane, R., and Caldeira, K.: Testing global ocean carbon cycle models using measurements of atmospheric O_2 and CO_2 concentration, Global Biogeochemical Cycles, 12, 213–230, 1998.

Suntharalingam, P. and Sarmiento, J.: Factors governing the oceanic nitrous oxide distribution: Simulations with an ocean general circulation model, Global Biogeochemical Cycles, 14, 429–454, 2000.

Thompson, R., Manning, A., Lowe, D., and Weatherburn, D.: A ship-based methodology for high precision atmospheric oxygen measurements and its application in the Southern Ocean region, Tellus, 59, 643–653, 2007.

Tohjima, Y., Machida, T., Watai, I., Akama, T., and Moriwaki, Y.: Preparation of gravimetric standards for measurements of atmospheric oxygen and reevaluation of atmospheric oxygen concentration, Journal of Geophysical Research, 110, D11 302, 2005.

Torres, R., Turner, D., Silva, N., and Rutllant, J.: High short-term variability of CO_2 fluxes during an upwelling event off the Chilean coast at 30° S, Deep-Sea Research I, 46, 1161–1179, 1999.

Trimmer, M., Chronopoulou, P.-M., Maanoja, S., Upstill-Goddard, R., Kitidis, V., and Purdy, K.: Nitrous oxide as a function of oyxgen and archaeal gene abundance in the North Pacific, Nature Communications, 7, 13 451, https://doi.org/10.1038/ncomms13451, 2016.

van der Plas, A., Monteiro, P., and Pascall, A.: Cross-shelf biogeochemical characteristics of sediments in the central Benguela and their relationship to overlying water column hypoxia, African Journal of Marine Science, 29, 37–47, 2007.

Veitch, J., Penven, P., and Shillington, F.: The Benguela: A laboratory for comparative modeling studies, Progress in Oceanography, 83, 296–302, 2009.

Walter, S., Bange, H., Breitenbach, U., and Wallace, D.: Nitrous oxide in the North Atlantic Ocean, Biogeosciences, 3, 607–619, https://doi.org/10.5194/bg-3-607-2006, 2006.

Wanninkhof, R.: Relationship Between Wind Speed and Gas Exchange Over the Ocean, Journal of Geophysical Research, 92, 7373–7382, 1992.

Wanninkhof, R.: Relationship between wind speed and gas exchange over the ocean revisited, Limnology and Oceanography: Methods, 12, 351–362, 2014.

Weiss, R.: Carbon Dioxide in Water and Seawater: The Solubility of a Non-Ideal Gas, Marine Chemistry, 2, 203–215, 1974.

Weiss, R. and Price, B.: Nitrous Oxide Solubility in Water and Seawater, Marine Chemistry, 8, 347–359, 1980.

Yamagishi, H., Tohjima, Y., Mukai, H., and Sasaoka, K.: Detection of regional scale sea-to-air oxygen emission related to spring bloom near Japan by using in-situ measurements of the atmospheric oxygen/nitrogen ratio, Atmospheric Chemistry and Physics, 8, 3325–3335, https://doi.org/10.5194/acp-8-3325-2008, 2008.

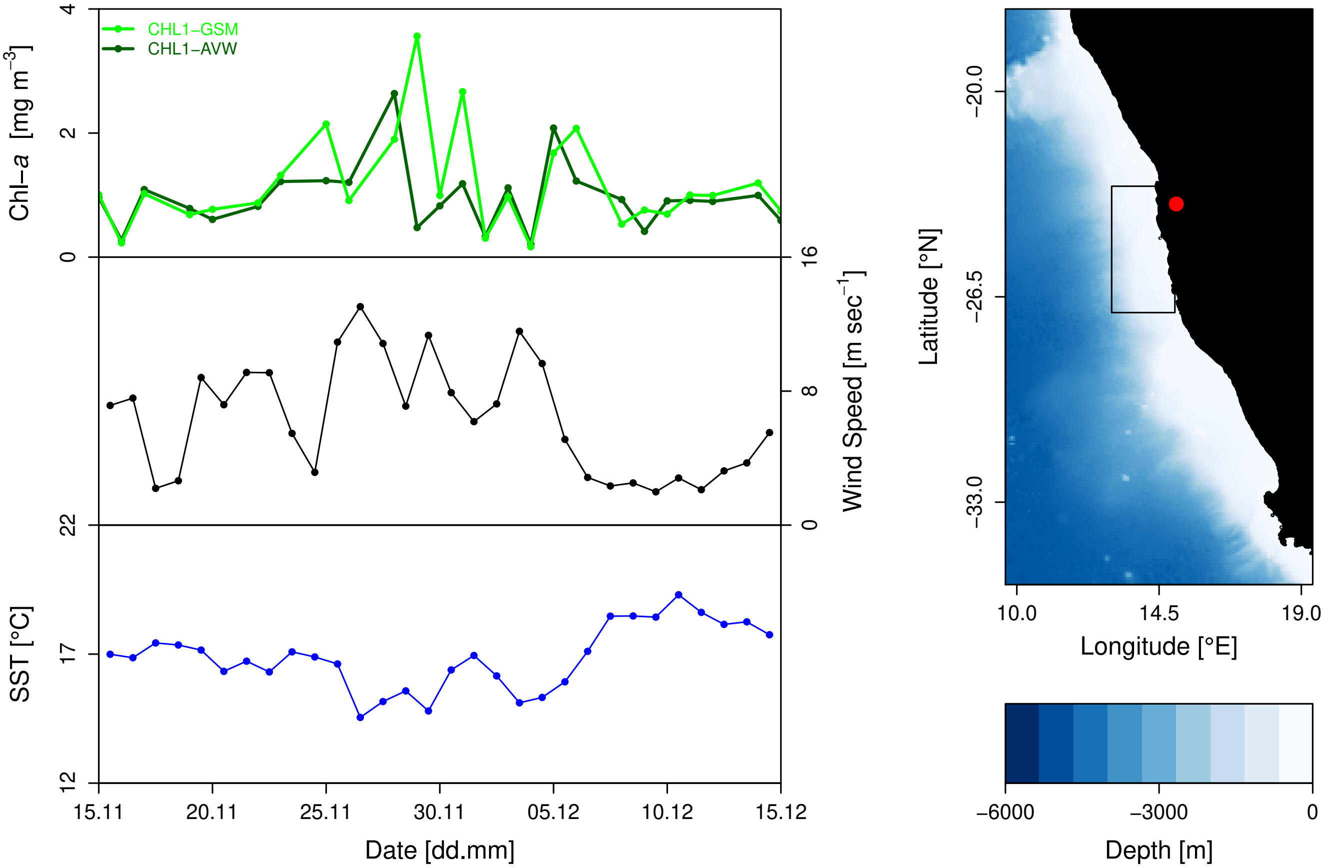

Figure 1. An example of an upwelling event at the end of 2013. The median chlorophyll *a* of the domain is shown over a period of one month, along with the domain-averaged 10-m wind speed and sea surface temperature (*left panel*). The Lüderitz/Walvis Bay domain is shown, overlain on a bathymetric map (*right panel*). Data is from Amante and Eakins (2009). Location of NDAO is given by a red dot.

Table 1. Means of All Atmospheric Anomalies and Top-Down Flux Density Estimates for Identified Upwelling Events

Species	Mean Anomaly $\pm 1\sigma$	Mean Flux Density $\pm 1\sigma$
CO_2	2.0 ± 1.1 ppm	0.64 ± 0.4 μmol m^{-2} sec^{-1}
$\delta(O_2/N_2)$, O_2	-85.1 ± 22.1 per meg	-5.5 ± 1.7 μmol m^{-2} sec^{-1}
APO, O_2	-76.1 ± 18.3 per meg	-5.1 ± 1.4 μmol m^{-2} sec^{-1}
N_2O	1.8 ± 0.7 ppb	0.57 ± 0.3 nmol m^{-2} sec^{-1}
CH_4	14.1 ± 17.3 ppb	4.3 ± 5.5 nmol m^{-2} sec^{-1}

Biogeosciences Discuss., https://doi.org/10.5194/bg-2019-103
Manuscript under review for journal Biogeosciences
Discussion started: 26 March 2019

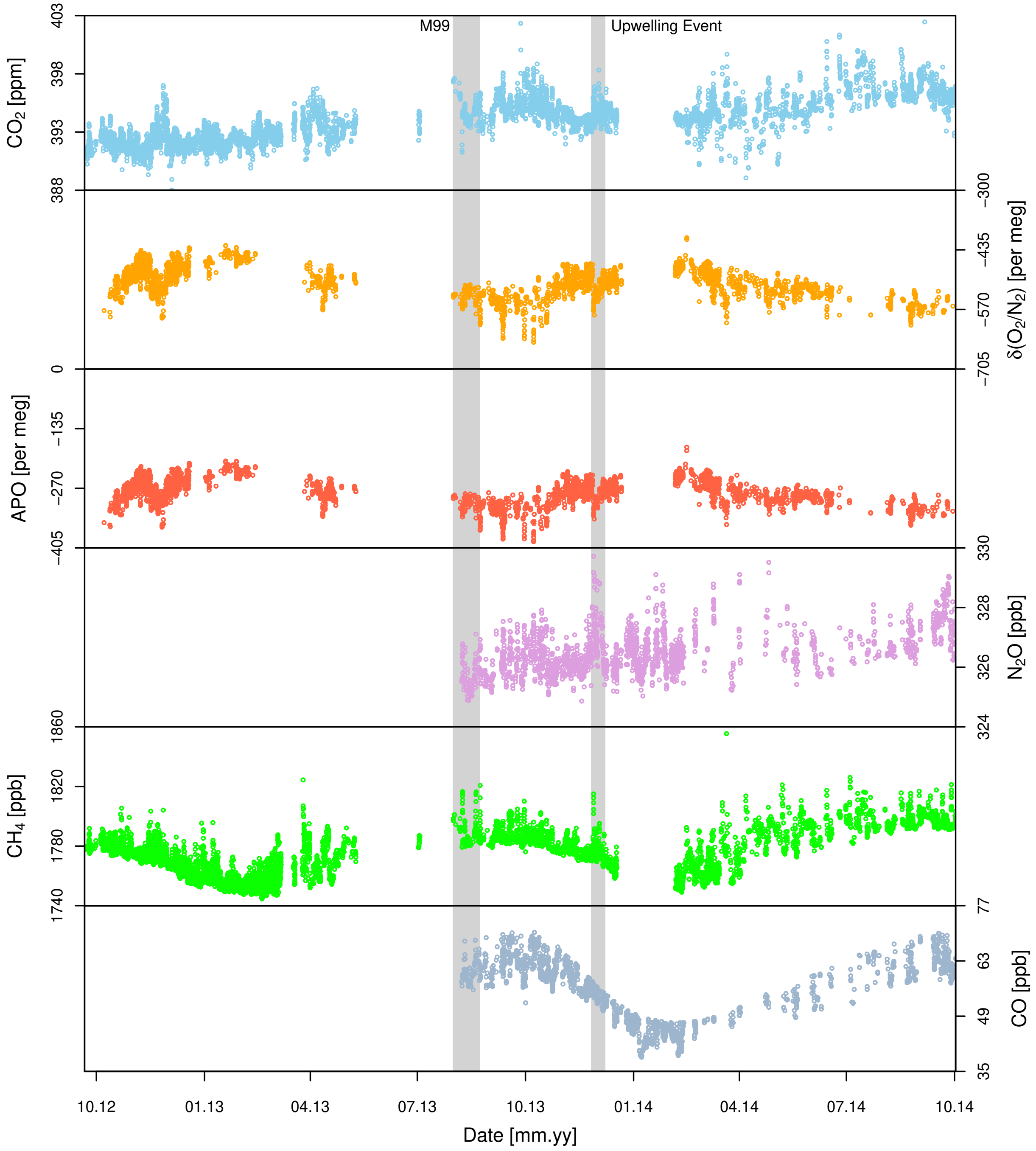

Figure 2. The NDAO time series, filtered based on back-trajectory and CO. The main measurands of the station are each plotted as 30 minute averages. The duration of M99 and the upwelling event discussed in the main text are both demarcated with gray rectangles and denoted with a label. The presence of an upper bound in the CO data is due to its use as a filtering criterion.

Biogeosciences Discuss., https://doi.org/10.5194/bg-2019-103
Manuscript under review for journal Biogeosciences
Discussion started: 26 March 2019

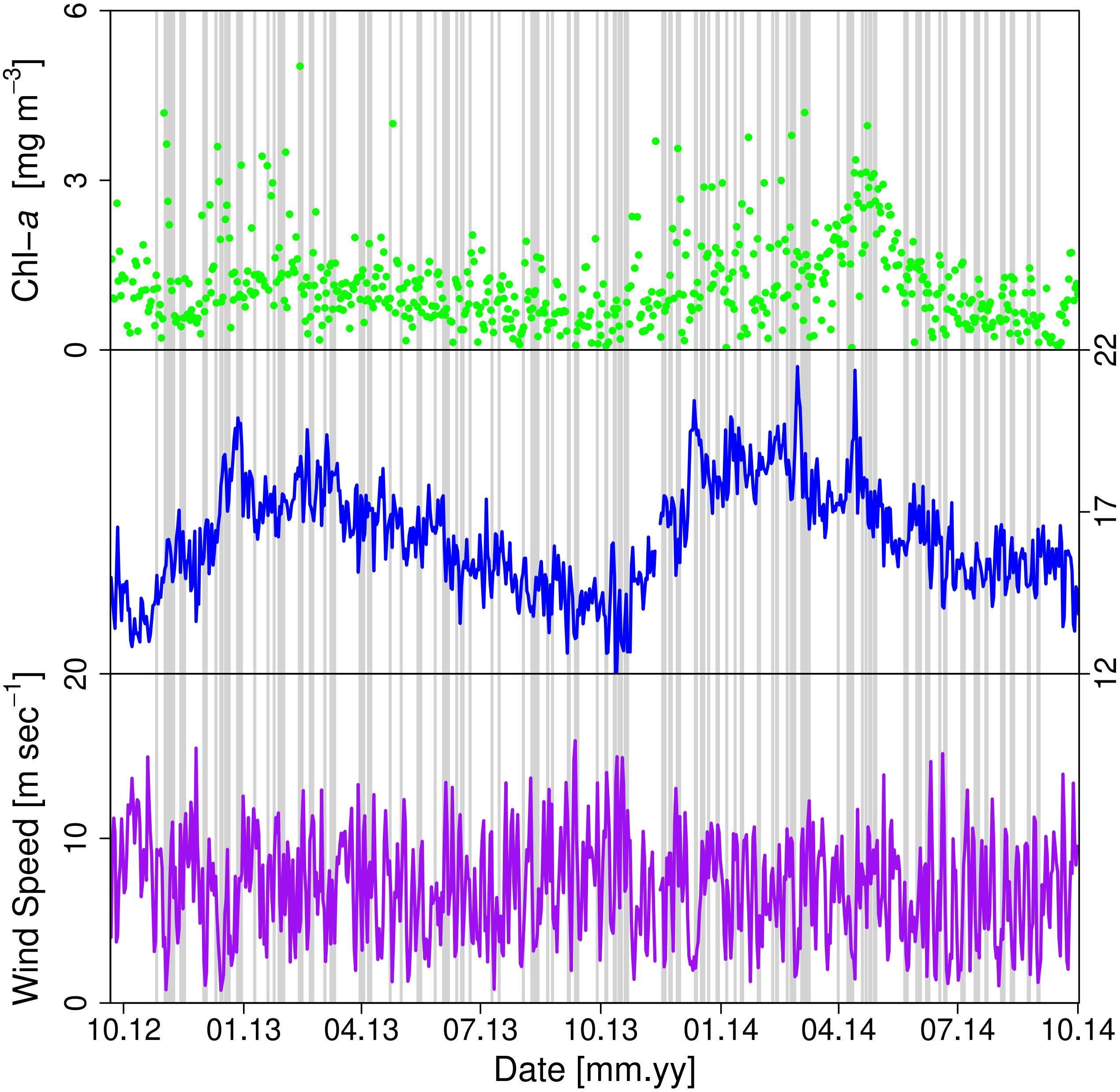

Figure 3. Surface chlorophyll a, temperature, and 10-m wind speed for the Lüderitz domain over the course of the two-year study period. Days which have been flagged as containing an upwelling event have been shaded.

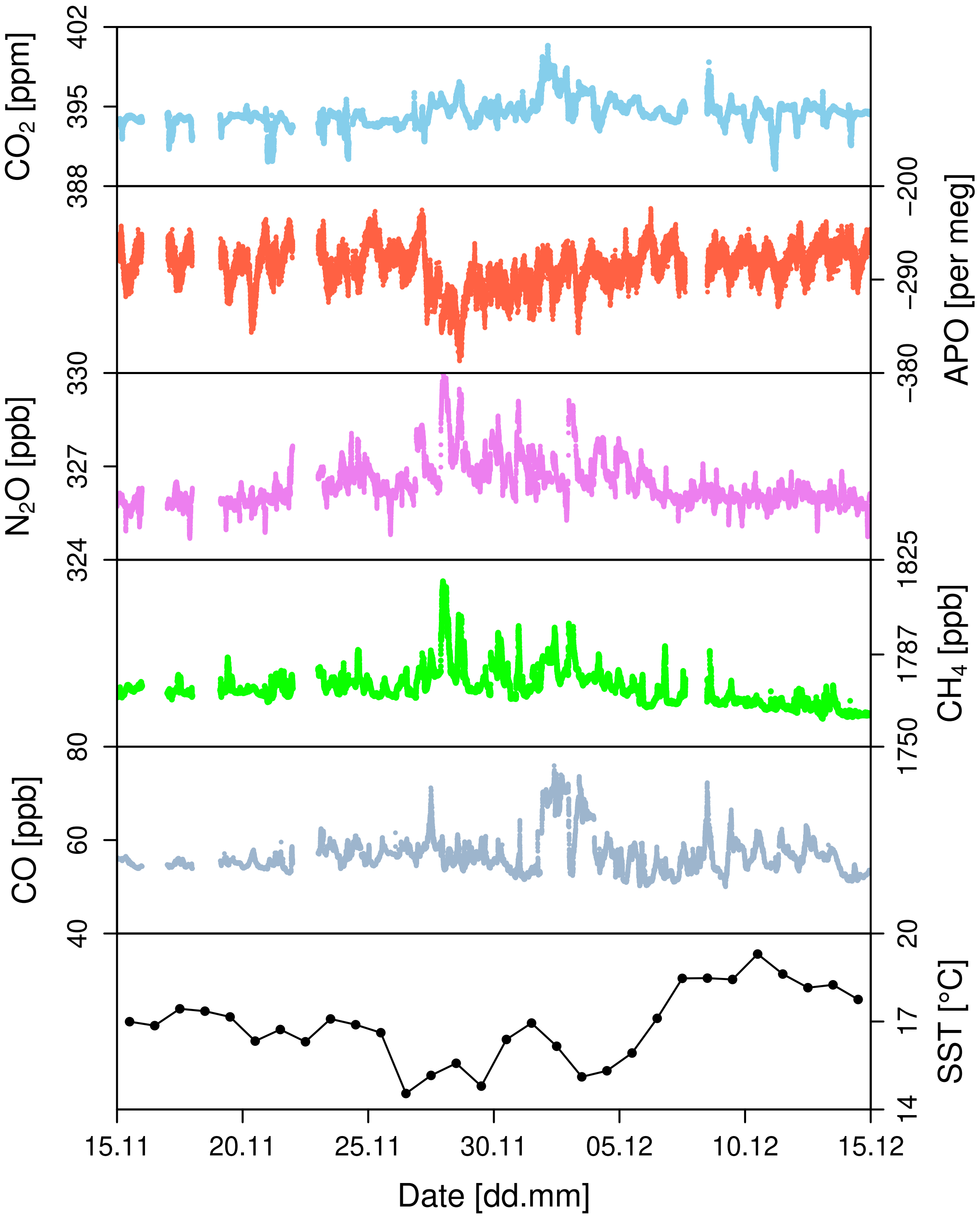

Figure 4. Atmospheric time series at NDAO throughout the upwelling event displayed in Figure 1.

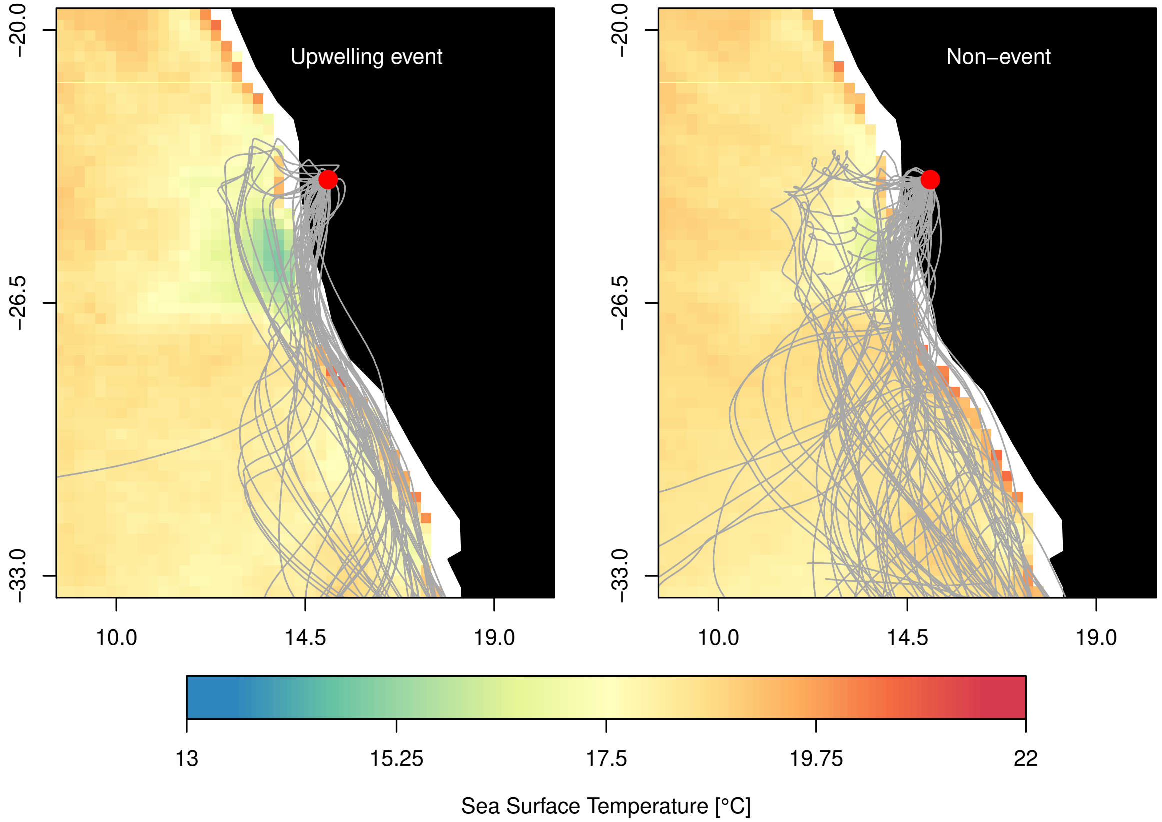

Figure 5. SST during (*left panels*) and preceding and after (*right panels*) the upwelling event described in Figure 2. The back-trajectories calculated for the respective periods are overlain. Location of NDAO given by a red dot.

Table 2. Comparison of Top-Down and Underway Flux Density Estimates for the M99 Upwelling Event (Aug 9 2013)

Species	Unit	Top-Down	Shipboard (k_{W92})	Shipboard (k_{N00})	Shipboard (k_{McG01})
CO_2	μmol m^{-2} sec^{-1}	0.59 ± 0.1	0.56 ± 0.2	0.43 ± 0.2	0.64 ± 0.2
$\delta(O_2/N_2)$, O_2	μmol m^{-2} sec^{-1}	-3.4 ± 0.3	-2.0 ± 0.6	-1.5 ± 0.5	-2.2 ± 0.7
N_2O	nmol m^{-2} sec^{-1}	0.43 ± 0.04	0.19 ± 0.1	0.14 ± 0.1	0.21 ± 0.1

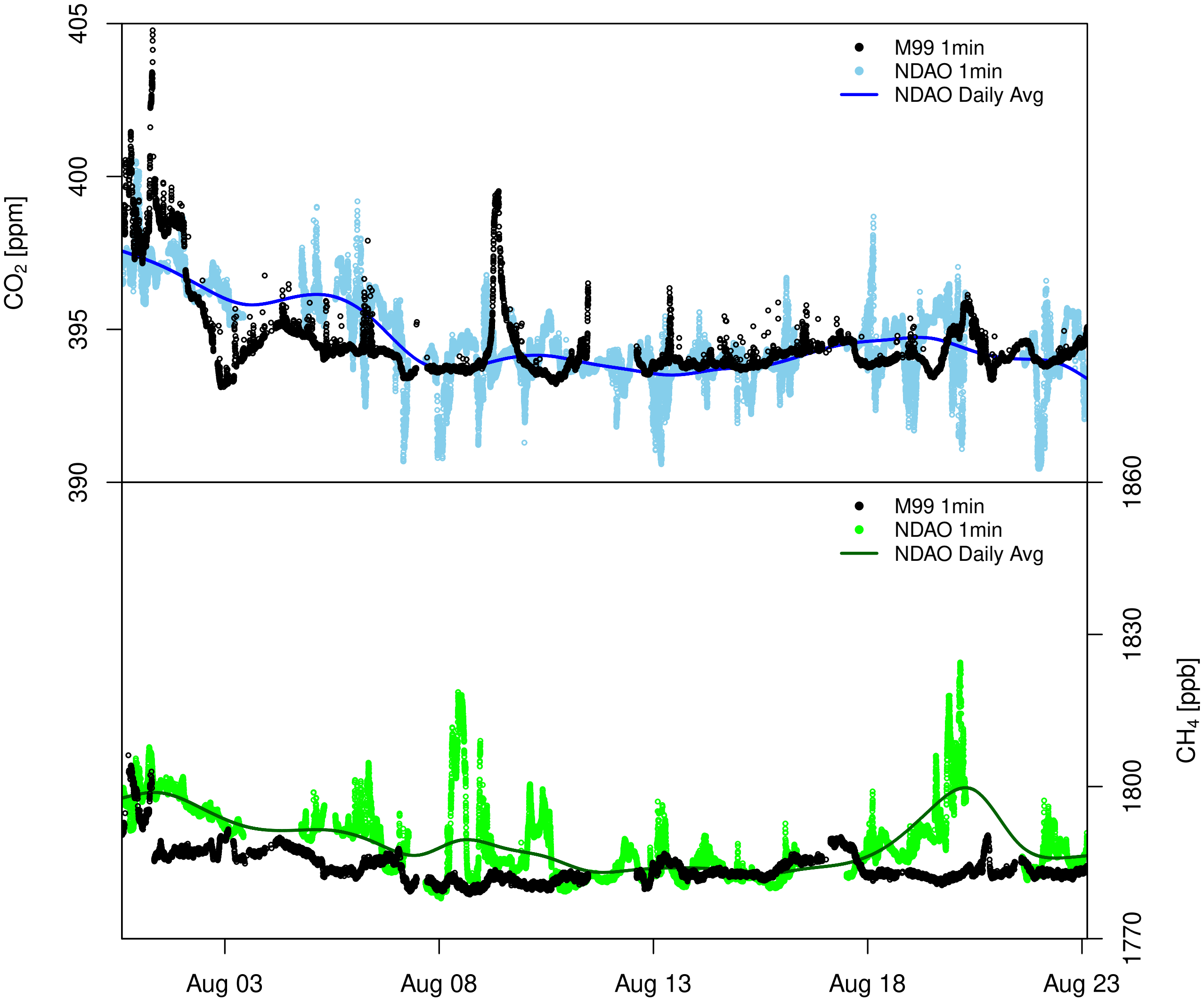

Figure 6. Atmospheric observations of CO_2 and CH_4 during the M99 cruise. Black points are the shipboard measurements and colored points are the NDAO measurements. Also shown for both species is a smooth fit to a rolling daily average. The diurnal variability was caused by a sea breeze/land breeze dynamic, with lower CO_2 mole fractions and higher CH_4 mole fractions occurring at night during the land breeze.

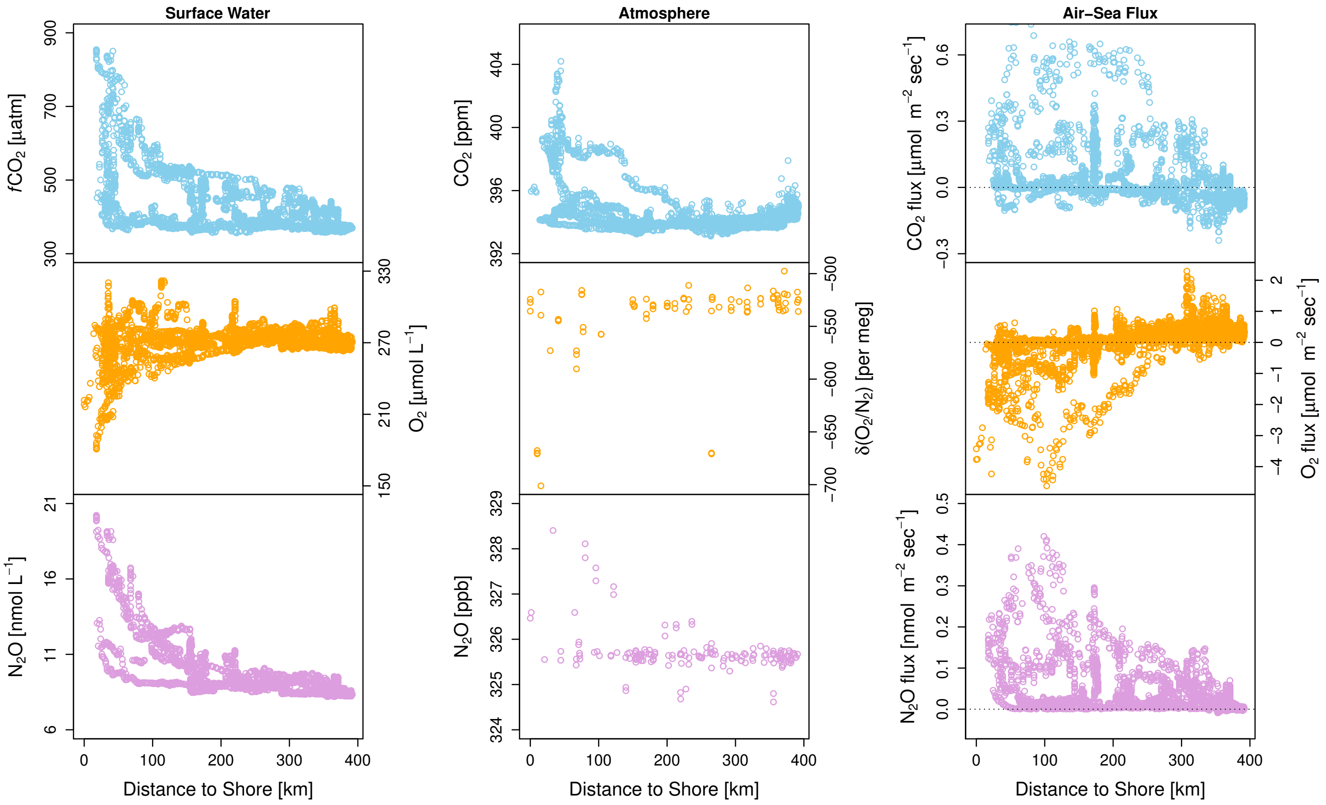

Figure 7. Air–sea flux densities for CO_2, O_2, and N_2O during M99 (*left panel*), the dissolved concentrations of the same species in surface water, ca. 6 m depth (*middle panel*), and the atmospheric abundance of all three species (*right panel*), all as a function of distance from shore. The dashed line on the rightmost panel indicates equilibrium between seawater and the atmosphere (i.e. no flux).

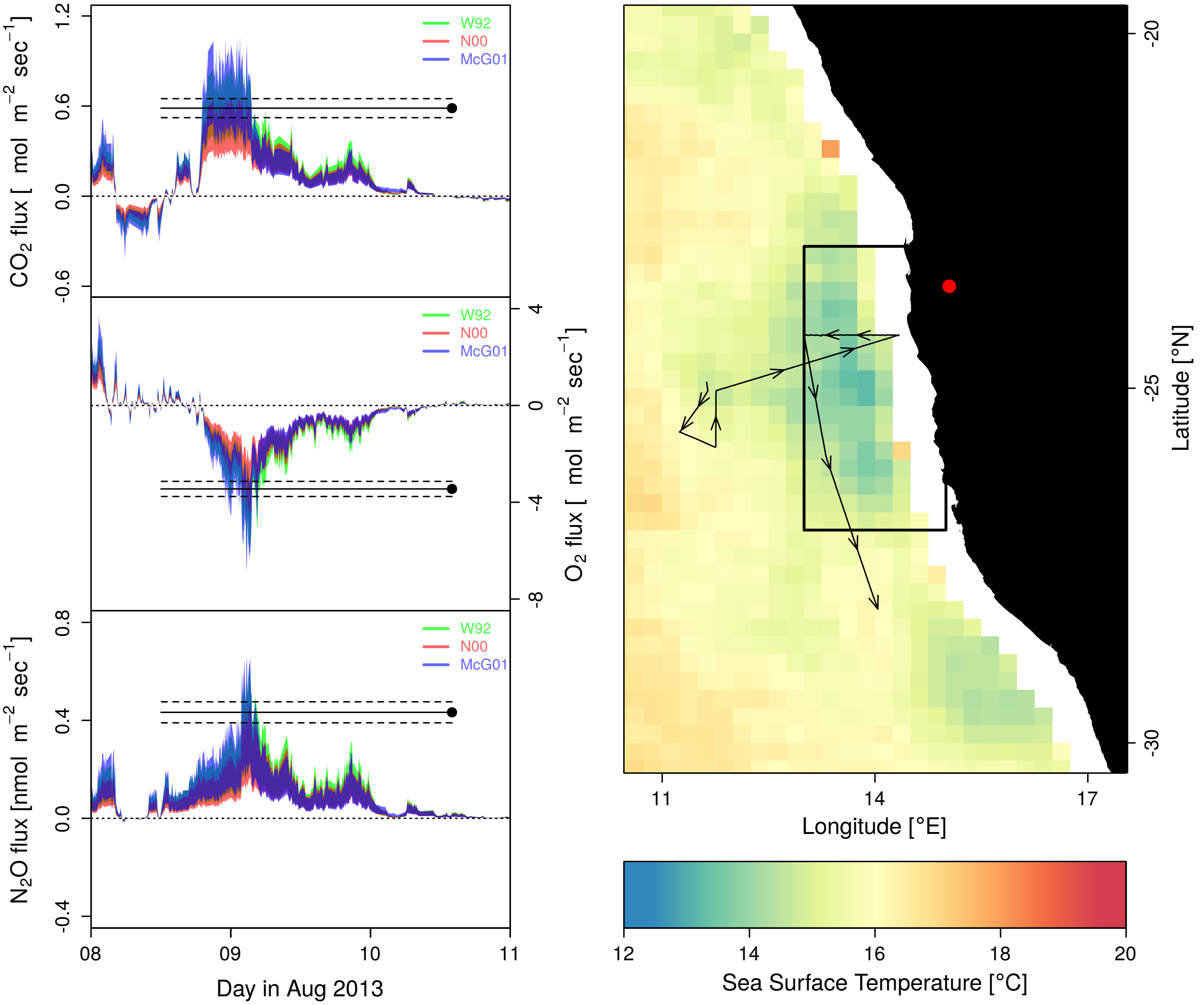

Figure 8. Air–sea flux densities for CO$_2$, O$_2$, and N$_2$O using bottom-up methods (*left panel*), with a shaded envelope depicting the estimated surface flux and its uncertainty. Three estimates are shown, each made with a different parameterization for k_w. A positive value indicates net evasion. W92, N00, and McG01 refer to the specific gas transfer velocity parameterization used. The top-down flux density estimate is plotted as a dot at the time of peak of the associated atmospheric anomaly. The horizontal line extending from each dot represents the time period during which the flux density associated with the anomaly was estimated to have occurred. Dotted lines indicate the uncertainty of the top-down estimate. Grid-cell average TRMM SST data for the three-day period is overlain with a cruise track and the Lüderitz/Walvis Bay domain (*right panel*). Location of NDAO is given by a red dot.

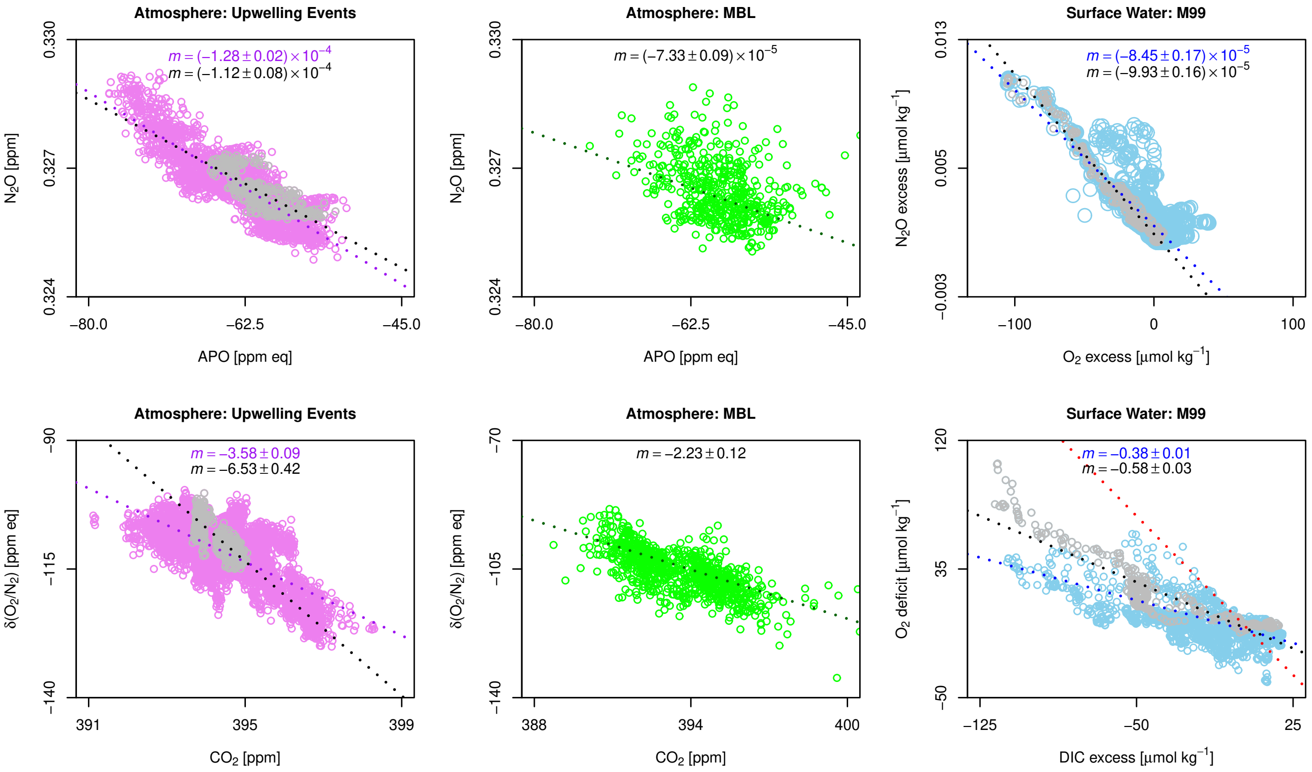

Figure 9. Comparison of the variability of O_2 with respect to N_2O and CO_2 with respect to O_2 at NDAO and in surface water. Displayed are the data corresponding to atmospheric anomalies associated with upwelling events (*left*), of all marine boundary layer air masses as selected by back-trajectories (*center*), and dissolved concentrations of CO_2, N_2O, and O_2 during M99 (*right*). Atmospheric O_2 is expressed as APO in ppm equivalents, and dissolved concentrations are expressed as the difference between the measured concentration and the concentration at saturation, *i.e.*, an excess, except for the bottom right panel, where it is shown as a deficit. In that plot, the Redfield ratio of 1.45 is plotted as a dotted red line for reference. Slopes (m) are given at the top of each plot. The gray symbols correspond with the upwelling event encountered during M99 (see Figure 8).